Phys Chem Minerals (2013) 40:51–62
DOI 10.1007/s00269-012-0546-4

ORIGINAL PAPER

Electrical conductivity of alkali feldspar solid solutions at high temperatures and high pressures

Haiying Hu · Heping Li · Lidong Dai · Shuangming Shan · Chengming Zhu

Received: 13 June 2012 / Accepted: 29 September 2012 / Published online: 13 October 2012

Abstract The electrical conductivities of alkali feldspar solid solutions ranging in chemical composition from albite ($NaAlSi_3O_8$) to K-feldspar ($KAlSi_3O_8$) were measured at 1.0 GPa and temperatures of 873–1,173 K in a multi-anvil apparatus. The complex impedance was determined by the AC impedance spectroscopy technique in the frequency range of 0.1–10^6 Hz. Our experimental results revealed that the electrical conductivities of alkali feldspar solid solutions increase with increasing temperature, and the linear relationship between electrical conductivity and temperature fits the Arrhenius formula. The electrical conductivities of solid solutions increase with the increasing Na content at constant temperature. At 1.0 GPa, the activation enthalpy of solid solution series shows strong dependency on the composition, and there is an abrupt increase from the composition of $Or_{40}Ab_{60}$ to $Or_{60}Ab_{40}$, where it reaches a value of 0.96 eV. According to these results in this study, it is proposed that the dominant conduction mechanism in alkali feldspar solid solutions under high temperature and high pressure is ionic conduction. Furthermore, since the activation enthalpy is less than 1.0 eV for the alkali feldspar solid solutions, it is suggested to be a model where Na^+ and K^+ transport involves an interstitial mechanism for electrical conduction. The change of main charge carriers can be responsible for the abrupt increase in the activation energy for $Or_{60}Ab_{40}$. All electrical conductivity data were fitted by a general formula in order to show the dependence of activation enthalpy and pre-exponential factor on chemical composition. Combining our experimental results with the effective medium theory, we theoretically calculated the electrical conductivity of alkali feldspar granite, alkali feldspar quartz syenite, and alkali feldspar syenite with different mineral content and variable chemical composition of alkali feldspar at high temperatures at 1.0 GPa, and the calculated results are almost in agreement with previous experimental studies on silicate rocks.

Keywords Alkali feldspar solid solutions · Electrical conductivity · Composition · High temperature · Conduction mechanism · Rocks

H. Hu · H. Li (✉) · L. Dai · S. Shan · C. Zhu
Laboratory for High Temperature and High Pressure Study of the Earth's Interior, Institute of Geochemistry, Chinese Academy of Sciences, Guiyang 550002, Guizhou, China
e-mail: HepingLi_2007@hotmail.com

Introduction

Electrical conductivity of minerals and rocks, which is one of the most important physical properties, can be used to explore the physical and chemical behavior of the Earth's interior (Omura et al. 1989; Constable 1990; Yoshino 2010; Yang et al. 2012; Yang 2012). On the other hand, the laboratory measurement of conductivity for rocks and minerals under high pressure and high temperature can provide significant constraints on the results of the inversion of magnetotelluric (MT) and geomagnetic depth sounding (GDS) and allows us to go further to estimate temperature, phase state, fluid content, and even mineralogy. Further, the electrical conductivity of minerals can help people to study the mineral microstructure, dynamics of charge transport, defect chemistry, and other mineral physical properties (Beekmans and Heyne 1976; Tyburczy and Fisler 1995).

Feldspars play an important role due to their widespread abundance in the Earth's upper crust and comprise about

50 wt% of the Earth's crust (Liu and Gorsey 2007). Feldspars are the major rock-forming minerals in magmatic, metamorphic, and sedimentary rocks; hence, their conductivity is likely to have large influence on electrical conductivity of rocks in the Earth's crust. The studies on the conductivity of alkali feldspar aid us to explore the electrical properties of the whole feldspar family. So far, laboratory electrical conductivity measurements on synthetic as well as natural feldspar have been extensively performed (Noritomi 1955; Khitarov and Slutskiy 1965; Mizutani and Kanamori 1967; Maury 1968a, b; Piwinskii and Duba 1974; Piwinskii et al. 1977; Guseinov and Gargatsev 2002; Bakhterev 2008). However, most of these previous studies on electrical conductivity of feldspar have been carried out at room pressure and high temperature. Only recently, Bagdassarov et al. (2004) estimated the pressure dependence of the glass transition temperature (T_g) from the pressure effect on the activation energy of electrical conductivity in albite, haplogranite, anorthite, and SiO_2 glasses. Later, Ni et al. (2011) measured the electrical conductivity of dry and hydrous albite glasses and liquids at high pressure and high temperature. Nevertheless, both of these samples that they used were feldspar glasses, not the natural crystalline feldspar commonly existing in the crust. Recently, Yang et al. (2012), Yang (2012) measured the electrical conductivity of dry and hydrous plagioclase at high temperature and pressure on both natural and pre-annealed samples from fresh mafic granulite xenoliths. But their sample was not alkali feldspar as we used. Most important of all, the influence of chemical composition on the electrical conductivity of feldspar has not been quantitatively evaluated. Although one important finding from these previous studies is that the conduction mechanism in feldspar is described as the migration of alkali cations (Na^+, K^+ and Ca^{2+}), it is still ambiguous that alkali cations transport by a vacancy process or by an interstitial one, which is also a controversial issue for alkali ions dynamics in the diffusion measurements of feldspar. Moreover, though the electrical conductivity of albite has been well studied in our previous work (Hu et al. 2011), these problems mentioned above have not been completely solved. Consequently, it is very important to clarify the dynamics of charge transport in alkali feldspar under high temperature. A systemic study of electrical conductivity of alkali feldspar with different composition at high temperature and high pressure is very significant.

In this study, we have measured the electrical conductivities of alkali feldspar solid solutions series (Or_xAb_{100-x}, $X = 20$, 40, 60, 80, and 100) at temperatures of 873–1,173 K and up to 1.0 GPa in the frequency range of 0.1–10^6 Hz using in situ AC complex impedance spectroscopy and a multi-anvil apparatus. The effect of chemical composition on electrical conductivity and activation enthalpy of alkali feldspar solid solutions is discussed in detail. Based on these results, we make a reasonable explanation for the conduction behavior of alkali feldspar under high temperature and high pressure.

Experimental procedures

Sample preparation

The natural low albite and K-feldspar, both from a large open ore feldspar deposit in Hengshan Mountain, Hunan province, China, were chosen to synthesize the solid solutions series. Table 1 shows the chemical composition of the two alkali feldspar end-members analyzed by EPMA-1600 electron probe at the State Key Laboratory of Ore Deposit Geochemistry, Institute of Geochemistry, Chinese Academy of Sciences, using natural minerals for standards. Standard operating conditions used were accelerating voltage of 25 kV and specimen current of 10 nA. Detailed analysis procedure and process are described in the (Zhong et al. 2009). The solid solutions series were prepared in the following way: both albite and K-feldspar were first ground into powder (<200 mesh) in an agate mortar. According to the mole fractions of albite and K-feldspar, the mixtures of two end-members were then weighed, thoroughly mixed in an agate mortar, and heated at 400 K for 12 h in order to remove the absorbed water. Then, the mixture powder was sealed in a copper capsule with a 0.025-mm-thick molybdenum (Mo) foil liner, which can avoid interdiffusion between the mixture sample and copper capsule at high temperature. The inner and outer diameters of the copper capsule were 8 mm and 9.5 mm, respectively, and the height was 20 mm, and the capsule was placed in a 32.5-mm edged cubic pyrophyllite with three-layer stainless steel sheets furnace. The temperature

Table 1 The chemical composition of the starting albite and K-feldspar analyzed by electron microprobe analysis (wt%)

Oxide	Albite	K-feldspar
SiO_2	68.54	64.57
Al_2O_3	19.40	18.28
Na_2O	11.50	0.09
K_2O	0.07	16.01
CaO	0.22	0
FeO	0.08	0.01
MgO	0.01	0
Cr_2O_3	0.11	0.22
TiO_2	0.04	0.01
BaO	0.02	0.04
Total	99.99	99.23

was controlled by a *Pt-PtRh*$_{10}$ thermocouple. The solid solutions synthesis was carried out at pressure of 1.0 GPa and temperature of 1,123 K in the YJ-3000t cubic-anvil high-press apparatus. The sintered time was about 48 h. At the end of the experiment, the sample was quenched by switching off the power to the heating circuit. Samples were taken out from the capsule and then cut into cylinders with the thickness of 3.0–6.0 mm and diameter of 6.0 mm for subsequent in situ electrical conductivity measurements. The powder X-ray diffraction of samples after the synthesis was performed in order to confirm solid solution phase. The chemical compositions of solid solutions samples after high-pressure synthesis are shown in Table 2 as Or_xAb_y, where x and y represent the mole fraction of K-feldspar and albite, respectively, to within 1 %. The preparation of K-feldspar for electrical conductivity measurement is similar to our previous experiments (Hu et al. 2011), in which the hot-press for albite was performed at 1,123 K and 1.5 GPa for 1 h.

Experimental method

The sample assembly for the electrical conductivity measurement is shown schematically in Fig. 1. The pressure-transmitting media was a 32.5-mm edged cubic pyrophyllite. To avoid the effect of pyrophyllite dehydration on the electrical conductivity measurements, the cubic pyrophyllite and end caps were heated at 1,173 K for 5 h in a muffle furnace prior to sample assembly. The heater was made of three-layer stainless steel sheets with a total thickness of 0.5 mm placed in the pyrophyllite block. The middle part of the assembly mainly consisted of aluminum oxide (Al_2O_3) and hexagonal boron nitride (HBN), which were directly in contact with the sample, in order to maintain the high degree of insulation under high temperatures and high pressures. In addition, a Ni shield, which was in contact with lead wire connected to ground, was installed between the aluminum oxide and boron nitride to effectively block external electromagnetic disturbance and to minimize the

Table 2 A summary of the sample composition and conditions for each impedance measurement; the results fit to $\sigma T = A\exp\left(-\frac{\Delta H}{kT}\right)$

Run	Composition	P (GPa)	T (K)	A (K·S/m)	ΔH (eV)	r^2
N100	Ab_{100}	1.0	873–1,173	12,930	0.84 ± 0.03	0.9932
H1064	$Or_{20}Ab_{80}$	1.0	873–1,173	12,414	0.86 ± 0.02	0.9961
H1623	$Or_{40}Ab_{60}$	1.0	873–1,173	9,897	0.87 ± 0.04	0.9909
H1706	$Or_{60}Ab_{40}$	1.0	873–1,173	21,037	0.96 ± 0.02	0.9969
H1707	$Or_{80}Ab_{20}$	1.0	873–1,173	21,365	0.99 ± 0.03	0.9962
K200	Or_{100}	1.0	873–1,173	13,508	0.99 ± 0.01	0.9989

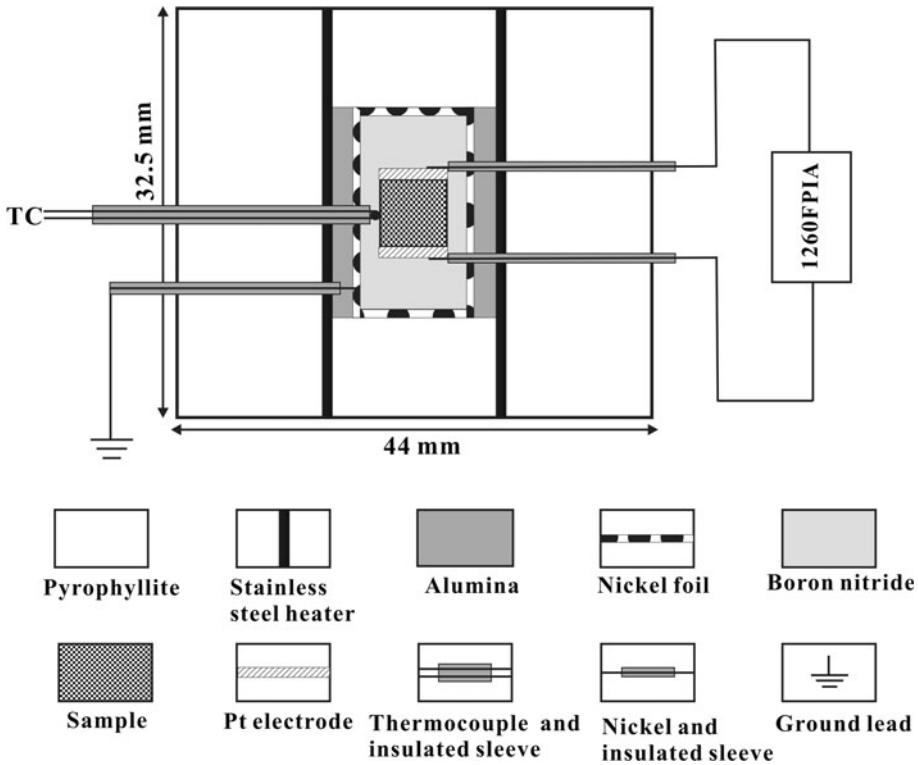

Fig. 1 Sample setup for electrical conductivity measurements

temperature gradient in the sample (Xu et al. 2000; Dai et al. 2008; Wang et al. 2010). The Pt disk electrodes with a thickness of 0.5 mm and diameter of 6.0 mm were placed on each end of sample, and a nickel–aluminum wire was connected with each electrode. Temperature was measured by a *Pt-PtRh*$_{10}$ thermocouple, the end of which was welded to a ball being in contact with the middle of the sample. After completing the sample assembly, it is heated 373 K in an oven overnight before electrical conductivity measurements. The pressure and temperature calibrations of the sample assembly are detailed in previous publications (Li et al. 1999; Liu et al. 2003; Shan et al. 2007).

The impedance spectra of the sample were collected using a Solartron 1260 Impedance/Gain Phase Analyzer in the frequency range of 0.1–10^6 Hz with the applied voltage of 1 V. The measurement procedure is as follows: the pressure was first raised to the designed value of 1.0 GPa with a compression rate of 0.2 kbar/min. The temperature slowly increased to 1,173 K with a rate of 20 K/min and held this temperature for 3 h in order to remove the absorbed water of sample assembly and to make the measurement system reach thermal transmission equilibrium in the sample cell. Then, the impedance spectra of the sample were frequently measured when temperature did not change any more; once it was reproducible, the impedance spectra of the sample were collected with the temperature interval of 50 K on cooling until temperature falling to 873 K. At the each temperature interval point, the system was stabilized for 15 min during which the ZPlot program repeatedly recorded the impedance spectra until it can overlap completely and no longer change any more. To check the reproducibility of the experimental data, the impedance spectra of $K_{0.8}Na_{0.2}AlSiO_4$ sample ($Or_{80}Ab_{20}$) were collected in a heating and cooling cycle so that we can estimate whether the time interval before data collection was enough or not for the sample to reach its thermodynamic equilibrium. For most of the other samples, the impedance spectra data were obtained in a cooling process. During measurement procedure, the errors of temperature and pressure in sample cell were about ±10 K and ±0.1 GPa, respectively (Liu et al. 2003; Dai et al. 2008).

Results

A typical result of complex impedance spectra for $K_{0.4}Na_{0.6}AlSiO_4$ sample ($Or_{40}Ab_{60}$) is shown in Fig. 2. The complex impedance spectra showed an ideal semicircular pattern in the frequency range of 0.1–10^6 Hz at experimental temperature. The semicircular arc represents the grain interior conduction (Roberts and Tyburczy 1991), but after the grain interior arc, neither a grain boundary arc nor a sample–electrode interface arc, which is caused by electrode polarization or by interaction between sample and electrode (Roberts and Tyburczy 1993; Huebner and Dillenburg 1995), appears in the plot. Consequently, grain boundary conduction does not contribute markedly to the electrical measurement, as previously reported for polycrystalline olivine, clinopyroxene, and garnet (Romano et al. 2006; Yang and Heidelbach 2012). All other samples with different composition in this study also exhibit the similar characteristics. Consequently, the equivalent circuit was composed of a resistor (R), and a capacitance (C) in parallel was chosen to fit the impedance spectra in the frequency range of 0.1–10^6 Hz, and all the errors of Zview program fitting are no more than 1.5 %. Then, the electrical conductivity of samples was calculated using the following equation:

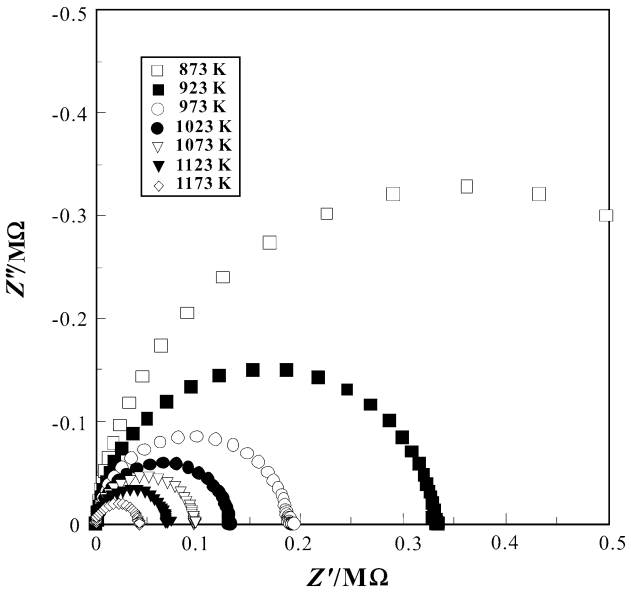

Fig. 2 Representative complex spectra of alkali feldspar solid solution ($Or_{40}Al_{60}$) at temperatures of 873–1,173 K and 1.0 GPa in the frequency range from 0.1 to 10^6 Hz. Z' and Z'' are the real and imaginary part of complex impedance, respectively

$$\sigma = \frac{1}{\rho} = \frac{l}{RS} \quad (1)$$

where l, S, and ρ are the sample length (m), cross-sectional area of the electrode (m^2), and resistivity of the sample (Ω m), respectively. The size of the sample was measured before and after impedance measurement and did not change during experimental process. Therefore, the error was mainly due to the fitting of impedance spectra, and the temperature error was due to the thermal gradient over the sample cell. The electrical conductivity values of alkali feldspar solid solution series, from the Zview program fitting of the collected impedance spectra and according to formula (1), are plotted in Figs. 3, 4, 5, and 6.

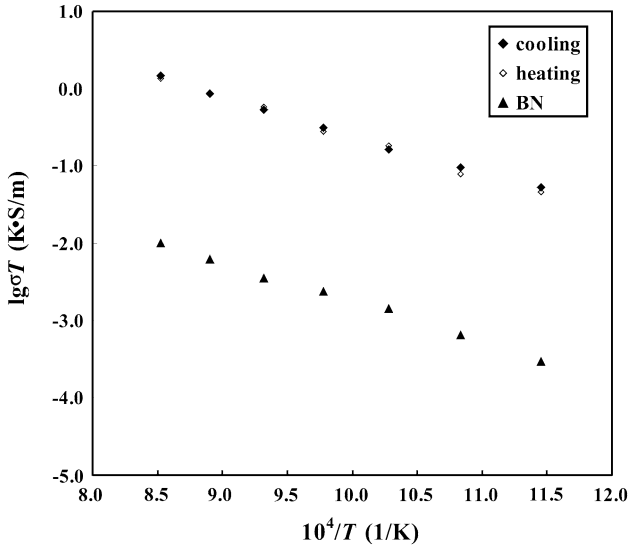

Fig. 3 Logarithm of electrical conductivity of alkali feldspar solid solution ($K_{0.8}Na_{0.2}AlSiO_4$) versus reciprocal temperature in heating (*open diamond*) and cooling cycles (*diamond*) at 1.0 GPa. Shown together is the conductivity of boron nitride at the same pressure

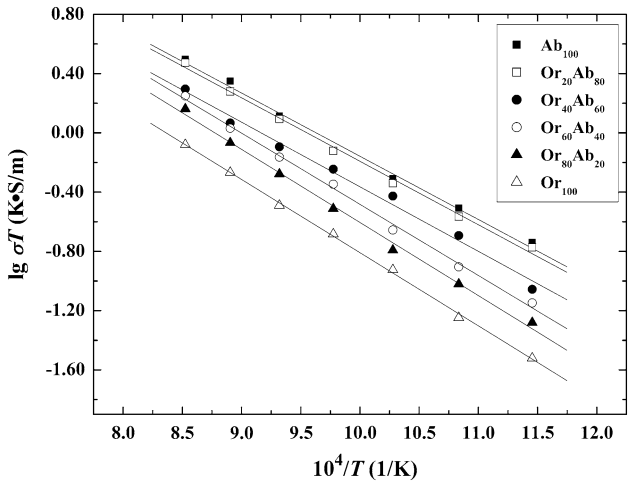

Fig. 4 Electrical conductivity (lg σT) of alkali feldspar solid solution series plotted as a function of reciprocal temperature (1/K) at 1.0 GPa

Figure 3 displays the logarithmic electrical conductivity of $K_{0.8}Na_{0.2}AlSiO_4$ sample versus reciprocal temperature in heating and cooling cycles at 1.0 GPa. We can see that the electrical conductivity of alkali feldspar solid solution in heating and cooling cycles is well reproducible, which means that the stabilization duration, 15 min, before each data collection was sufficient for both thermal transfer and thermodynamic state of charge carriers inside the sample to reach their respective equilibrium. Moreover, the background conductivity was measured in order to examine the insulation of the alkali feldspar sample surroundings. We used HBN to replace the sample and collected its impedance spectra at the same pressure and temperatures as in the

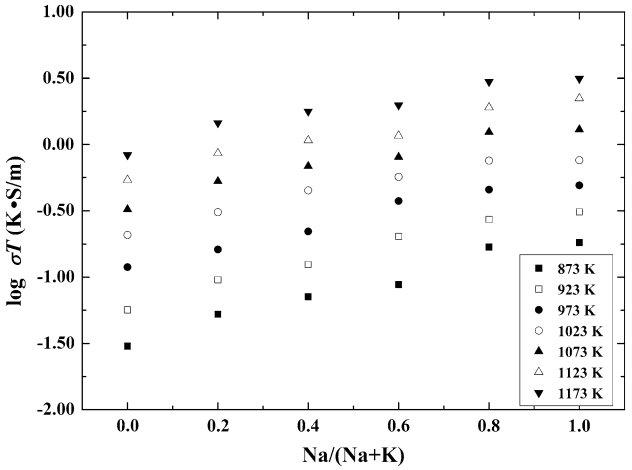

Fig. 5 Electrical conductivity (lg σT) of alkali feldspar solid solutions plotted as a function of Na/(Na + K) under conditions of 873–1,173 K and 1.0 GPa

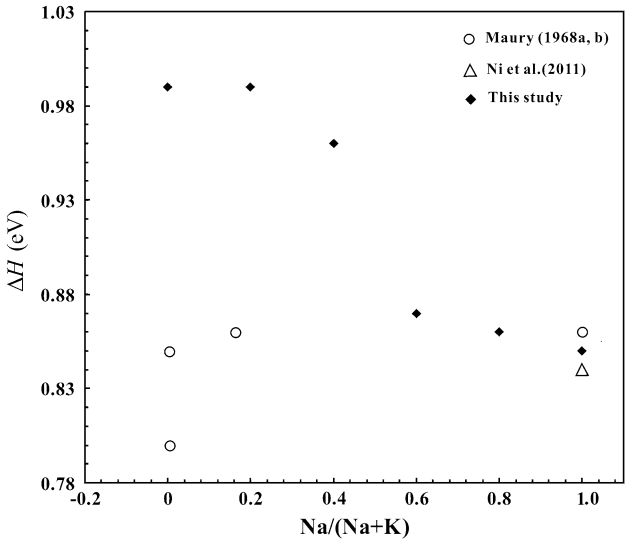

Fig. 6 Activation enthalpy for the electrical conductivity in alkali feldspar solid solutions plotted as a function of Na/(Na + K) at 1.0 GPa. Also shown are data for albite glasses (*open triangle*) from Ni et al. (2011) and for natural alkali feldspar (*open circle*) from Maury (1968a, b)

alkali feldspar sample experiment. The result shows that the electrical conductivity of HBN was two or more orders of magnitude lower than that of the $K_{0.8}Na_{0.2}AlSiO_4$ sample, which implies, by using HBN as insulation medium, our alkali feldspar samples could acquire good insulation surroundings in the impedance spectra measurement experiments. In fact, as an ideal insulation medium (Eichler and Lesniak 2008), BN has also been widely used by many authors in electrical measurement experiments (Fuji-ta et al. 2004, 2007; Ni et al. 2011; Yang et al. 2012; Yang 2012; Yang and Heidelbach 2012).

The logarithms of the products of electrical conductivities and temperatures at 1.0 GPa and 873–1,173 K were plotted against the reciprocal temperatures in Fig. 4. Through linear fitting to the data points at different temperature, we obtained the linear correlation coefficients no less than 0.9909; hence, the electrical conductivity of alkali feldspar solid solutions can be expressed by an Arrhenius formula:

$$\sigma T = A\exp(-\Delta H/kT) \quad (2)$$

where A, ΔH, k, and T are the pre-exponential factor (K S/m), activation enthalpy (eV), Boltzmann constant (eV/K), and absolute temperature (K), respectively. The Arrhenius fitting parameters were obtained by calculating the slope and intercept of the straight lines displayed in Fig. 4 and are given in Table 2. In Fig. 4, the logarithmic conductivity of alkali feldspar linearly increases with the decreasing reciprocal temperature. The electrical conductivity appears to be very sensitive to composition along the albite–K-feldspar join and increases with the increase in albite content at constant temperature. For example, the electrical conductivity of albite (Ab_{100}) is about 0.6 log units higher than that of K-feldspar (Or_{100}) at 1,173 K, and the discrepancy becomes larger and larger with the decrease in temperature.

Figure 5 shows the electrical conductivity of alkali feldspar solid solutions as a function of Na/(Na + K) over the experimental temperature range at 1.0 GPa. The relative small variation in bulk chemical composition can result in notable change in electrical conductivity for alkali feldspar. Each data set at each given temperature shows a near-linear increase in the electrical conductivity with the increasing ratio of Na/(Na + K), implying a positive dependence of conductivity on the Na concentration in alkali feldspar.

The activation enthalpy (Table 2) is plotted against chemical composition in Fig. 6, in which some previous results are also shown. Interestingly, the activation enthalpy of alkali feldspar is strongly dependent on the composition, and there is an abrupt increase in the activation enthalpy when the concentration of potassium ions is higher than that of sodium ions in alkali feldspar.

Discussions

Comparison with previous studies

Since the present study is the first to provide data on the electrical conductivity of alkali feldspar solid solutions, we choose some representative data, in which the chemical composition of alkali feldspar is similar to ours, to compare as shown in Fig. 7. Khitarov and Slutskiy (1965) measured

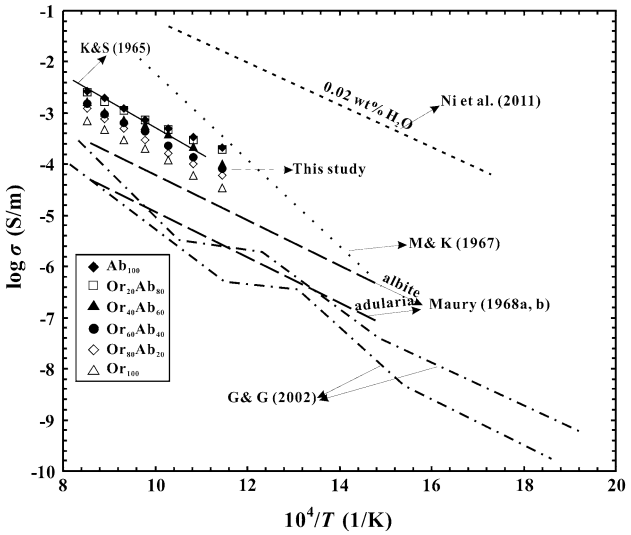

Fig. 7 Comparison of electrical conductivity of alkali feldspar by the present work with that by previous studies. *Solid line* albite (An_3Ab_{97}), 1.0 GPa, DC method, by Khitarov and Slutskiy (1965); *dotted line* single-crystal alkali feldspar (61 % orthoclase, 34 % albite, and 5 % anorthite), ambient pressure, AC method, by Mizutani and Kanamori (1967); *long-dashed line* adularia ($K_{0.84}Na_{0.16}AlSi_3O_8$), ambient pressure, AC method, by Maury (1968a, b); *dotted-dashed line*: natural microcline, ambient pressure, DC method, by Guseinov and Gargatsev (2002); *short-dashed line* dry albite glass, 1.8 GPa, AC method, by Ni et al. (2011)

the electrical conductivity of a polycrystalline albite (An_3Ab_{97}) prior to melting at 0.28 GPa. Our results for the Na-rich alkali feldspar are generally in agreement with theirs; however, our activation enthalpy (0.84 eV) was much lower than that (~1.02 eV) of Khitarov and Slutskiy (1965). The discrepancy might be attributed to the different chemical composition of samples. The sample (An_3Ab_{97}) from Khitarov and Slutskiy (1965) contains a few calcium ions, of which the ionic radius and charge are larger and higher than those of sodium ions, respectively. Because of the incorporation of calcium ions in framework structure, the average Na–Na distance increases, and the energy barrier for a jump of Na from one site to another also increases, which results in the increase in the activation enthalpy.

Mizutani and Kanamori (1967) measured the single crystal alkali feldspar with the composition of 61 % orthoclase, 34 % albite, and 5 % anorthite using DC method at room pressure and high temperature. Their results are obviously higher than ours, including the activation energy (1.65 eV). In addition, Guseinov and Gargatsev (2002) also used DC method to measure the electrical conductivity of two natural single crystal microclines with a minor albite, and our results are obviously higher than theirs. The discrepancy in the results of Guseinov and Gargatsev (2002) and ours could be mainly due to the difference in respective measurement methods.

The DC method usually leads to serious polarization of sample due to the existence of a large number of lattice defects and their orientation in the sample under the applied direct-current field. Orientation polarization of lattice defects would weaken the effective electrical field applied on the charge carriers, and reduce the driving force of the charge carriers and the total current of the measuring circuit; therefore, the measured conductivity will be lower than the true values. Another possible reason for the discrepancy is the difference in sample preparation. Both Mizutani and Kanamori (1967) and Guseinov and Gargatsev (2002) used the natural single-crystal samples. By contrast, our samples are solid solution samples, which can avoid the influence of anisotropy on the results. A lot of experimental reports have shown that the electrical conductivity of single crystal for many minerals such as enstatite, quartz, and pyroxene is highly anisotropic (Duba et al. 1973; Dvorák and Schloessin 1973; Dai and Karato 2009a; Wang et al. 2010). In addition, according to the diffusion data of alkali feldspar obtained by Christoffersen et al. (1983), the diffusion rates of alkali ions are largely different in different crystallographic directions. Therefore, it is suggested that the electrical conductivity of alkali feldspar is also anisotropic.

Maury (1968a, b) determined the electrical conductivity of natural albite and adularia ($K_{0.84}Na_{0.16}AlSi_3O_8$) at 673–1,173 and ambient pressure using AC impedance spectroscopy method. The electrical conductivity of albite glass with 0.02 wt% H_2O, which was performed by Ni et al. (2011) at 473–1,773 K and high pressure using the same experimental method, is also compared to ours as shown in Fig. 7. The obvious difference may be explained as follows: (1) The sample of Maury (1968a, b) was single-crystal sample. As we discussed above, the crystallographic directions have an important influence on the electrical conductivity of minerals. (2) The different lattice structures of respective samples can also explain the different conductivities. Lattice structure is one of the important factors that significantly affect the electrical conductivity of materials. The single-crystal adularia is usually composed of a mixture of monoclinic and triclinic crystalline domains (Zhou et al. 2001), and the structure of glass including the albite glasses is somewhat analogous to that of liquid and is random networks and any long-distance periodicity is lacking, whereas our samples are solid solutions. Therefore, the different lattice structures among the respective sample can lead to different experimental results. (3) A small quantity of water content in the sample of Ni et al. (2011) can also enhance electrical conductivity.

Conduction mechanisms of alkali feldspar

Since the plot of log σT versus T^{-1} yield one linear response over the experimental temperature range, there is only one conduction mechanism for alkali feldspar solid solutions. The dominant conduction mechanism is ionic conduction and the charge carriers are Na^+ and K^+, as also suggested for feldspar minerals and feldspar glasses in previous electrical conductivity experiments and diffusion experiments (Maury 1968a, b; Lin and Yund 1972; Behrens et al. 1990; Eldin and Alaily 1998; Guseinov and Gargatsev 2002; Bagdassarov et al. 2004; Ni et al. 2011; Yang et al. 2012). Large numbers of studies show that the migration of ions in minerals is controlled by many factors, such as anion porosity of the structure, electrostatic site energy, and size of the ion (Dowty 1980; Henderson et al. 1985). Feldspars have particular structure in which the tetrahedrons of SiO_4 and AlO_4 connect at each corner to other tetrahedrons forming an intricate, three-dimensional, negatively charged framework, and these cations (K^+, Na^+, Ca^{2+}) occupy the voids in the structure; hence, the anion porosity of feldspar is relatively higher than the porosity of other minerals, for example, the anion porosities of albite and orthoclase are 49.7 and 53.8 %, respectively, whereas those of calcite and forsterite are 48.9 and 46.4 %, respectively (Dowty 1980). As Dowty (1980) mentioned that the increase in porosity in silicates with increasing degree of linkage (polymerization) of silicon–oxygen tetrahedral implies that the decrease in the average coordination number of cations and the lower coordination number usually results in looser packing. Consequently, the looser structure of feldspars can provide advantage in the migration of alkali cations (K^+, Na^+) in the crystal lattice. Additionally, the site energy of Na^+ and K^+ is in the range of 11–13 eV, which is far lower than that of O^{2-} (50–63 eV), Al^{3+} (105 eV), Si^{4+} (176–197 eV) (Ohashi 1976). Although the ionic radius of alkalis is relatively larger than that of other ions in the tetrahedron, the lower site energies of alkalis and the higher porosities of feldspars evidently compensate for the larger size of alkali ions. Therefore, Na^+ and K^+ are extremely mobile elements compared with other ions such as O^{2-}, Al^{3+} and Si^{4+} normally located in tetrahedral sites.

Other candidates that could act as charge carriers such as electrons and protons are not likely to play a role in electrical conduction. In general, electronic conductivity occurs in iron-bearing minerals such as olivine, clinopyroxene, orthopyroxene, and garnet, through small polaron hopping between ferrous and ferric ions (Dai and Karato 2009b, c; Yoshino et al. 2009, 2011, 2012; Farla et al. 2010; Poe et al. 2010; Yang et al. 2012; Yang 2012; Yang and Heidelbach 2012). For our samples, the very low iron content precludes any significant electronic conduction. It is also impossible for protons to be the dominant charge carrier in our sample, since the activation enthalpy displays obvious dependency on the alkali ions content of alkali feldspar as shown in Fig. 6. On the basis of above analysis,

Na^+ and K^+ are the most likely candidates to act as charge carriers in alkali feldspars due to their high diffusivity.

So far, the transport mechanism of alkali ions is still controversial as to whether the migration of alkalis involves a vacancy mechanism or an interstitial one. In a conduction process, alkali ions jump from an initial site to a nearby defect along the applied electrical field direction by thermal activation. If the defects are interstitial positions (not charged), the change in defect concentration with temperature is negligible, and the measured activation enthalpy is simply associated with the motion of mobile species. Therefore, the activation enthalpy is

$$\Delta H = \Delta H_{mi} \tag{3}$$

where ΔH_{mi} is the energy for charge carriers moving to the interstitial position.

If the defects are vacancies (charged), the molar fraction of defects N_v varies with temperature, and the measured activation enthalpy consists of formation enthalpy for vacancies ΔH_f and vacancy motion enthalpy ΔH_{mv}. Thus,

$$\Delta H = \frac{1}{2}\Delta H_f + \Delta H_{mv} \tag{4}$$

since ΔH_{mi} and ΔH_{mv} have very similar values and ΔH_f is normally much larger than migration enthalpy (ΔH_m); the activation enthalpy for vacancy mechanism is far higher than that of an interstitial mechanism. According to the lower activation energies (less than 1.0 eV) obtained in this study and previous studies as shown in Fig. 5, it is proposed that the migration of Na^+ and K^+ involves an interstitial mechanism in alkali feldspar. The formation of Frenkel defects can be written as

$$Na^X_{A_1} = Na^{\cdot}_i + V'_{A_1} \tag{5}$$

$$K^x_{A_1} = K^{\cdot}_i + V'_{A_1} \tag{6}$$

where $Na^x_{A_1}$ and $K^X_{A_1}$ are sodium and potassium ions located in their normal lattice sties of A_1, $Na^{\cdot}_i$ and $K^{\cdot}_i$ are sodium and potassium ions occupying the interstitial sites, respectively; and V'_{A_1} is the vacancy of alkali ions in their normal lattice sites of A_1. At high temperatures, the Na^+ and K^+ jump from their normal lattice sites to their adjacent interstitial sites along the electrical field direction and leave vacancies behind them.

Combing the low activation energy in this study with the theoretically calculated interstitial migration energy of alkali ions in alkali feldspar, the interstitial mechanism is also strongly supported. Jones et al. (2004) obtained the interstitial migration energy for Na^+ and K^+ in albite and K-feldspar by theoretical calculation, and the activation energies of interstitial migration for K^+ and Na^+ are 1.86 and 1.31 eV in albite, respectively, and 0.99 and 0.70 eV in K-feldspar, respectively. The activation enthalpy (0.84) of albite in this study is much lower than that (1.31 eV) of Jones et al. (2004). The discrepancy in the calculated structure carried out by Jones et al. (2004) could account for the difference between the experimentally determined and calculated activation energy for albite. However, the activation enthalpy of 0.99 eV for K-feldspar in our study is identical to that of Jones et al. (2004). Consequently, our activation enthalpy data can also provide significant evidence to support the interstitial migration mechanism for Na^+ and K^+ in alkali feldspar.

Therefore, the variation in activation enthalpy with chemical composition as shown in Fig. 6 can be reasonably explained. When the value of Na/(Na + K) is no less than 0.6, the activation enthalpy is no more than 0.87 eV and smoothly increases with the decreasing content of Na^+. Although a few K^+ are contained in Na-rich alkali feldspar solid solutions, Na^+ is still suggested to be the major charge carriers. The small increase in activation enthalpy is due to the increase in average Na–Na distance with the increasing concentration of K^+, and the energy barrier for a jump of Na^+ from one site to another increases. When the content of K^+ is higher than that of Na^+, the activation enthalpy abruptly increases to 0.96 eV, and the likely explanation is that K^+, with relatively high activation energy, takes part in the electrical conduction and becomes a major charge carrier. However, Na^+ can also contribute to the electrical conduction for alkali feldspar solid solutions except the end-member K-feldspar.

Effect of chemical composition on electrical conductivity

The present study shows that the electrical conductivities of alkali feldspar solid solutions exhibit strong composition (Na/(Na + K)) dependence, as seen in studies concerning electrical conductivity of iron-bearing silicates as a function of Mg/(Mg + Fe) for olivine (Omura et al. 1989; Hirsch et al. 1993; Yoshino et al. 2012), pyroxenes (Seifert et al. 1982), garnet (Romano et al. 2006), and ringwoodite (Yoshino and Katsura 2009). As shown in Fig. 6, activation enthalpies were seen to decrease with the rise in Na/(Na + K), which is closely related to a decrease in average Na–Na distance. Similar relation was also observed for iron-bearing minerals as a function of Mg/(Mg + Fe) (Romano et al. 2006; Yoshino and Katsura 2009; Yoshino et al. 2012). The relationship between activation enthalpy and composition can be approximated at given pressure by the following equation.

$$\Delta H = \Delta H_0 + \beta(X_{Na/(Na+K)})^{\gamma} \tag{7}$$

where ΔH is the activation enthalpy at a specific $X_{Na/(Na+K)}$, ΔH_0 is the activation enthalpy observed at very low Na concentrations, $X_{Na/(Na+K)}$ is the ratio of Na/(Na + K),

and β and γ are constants that account for geometrical factors, respectively. In consideration of the discontinuous variation in activation enthalpy (Fig. 6), the relationships between activation enthalpy and $X_{Na/(Na+K)}$ are well fitted by Eq. (7) for Na-rich ($X_{Na/(Na+K)} > 0.5$) and K-rich ($X_{Na/(Na+K)} < 0.5$) compositions, respectively. The fitting parameters are shown in Table 3.

Since the concentration of alkali ions controls the conductivity variation in alkali feldspar solid solutions, and its dependence on the pre-exponential factor, the resultant electrical conductivity of alkali feldspar solid solutions, excluding the end-member K-feldspar, can be described as follow:

$$\sigma T = \sigma_0 X^{\alpha}_{Na/(K+Na)} \exp\left(-\frac{\Delta H_0 + \beta X^{\gamma}_{Na/(Na+K)}}{kT}\right) \quad (8)$$

where σ_0 is the pre-exponential factor for ionic conduction and α is a constant. According to Eq. (8), the present data for Na-rich and K-rich alkali feldspar solid solutions are separately fitted by using the global least-squares fitting, and the relevant parameters for alkali feldspar solid solutions are summarized in Table 3. Using these parameters and Eq. (8), the calculated conductivity values and activation enthalpy are in good agreement with the experimental values.

Geophysical implications

Laboratory electrical conductivity results of minerals at high temperature and high pressure can provide reliable database for establishing the electrical conductivity of rocks by using the conduction models of mixture. So far, a number of electrical conductivity models of binary solid mixtures have been developed, such as the series and parallel (SP) solutions (Schulgasser 1976), the geometric mean (GM) model (Shankland and Duba 1990), the Hashin–Shtrikman (HS) model (Hashin and Shtrikman 1962), the effective conductivity (EC) model (Del Rio et al. 1998), and effective medium (EM) model (Landauer 1952). Since EM model is the only average to fit between HS bounds which are the narrowest restriction as previous publications reported (Xu et al. 2000; Dai et al. 2012), it is chosen in this study to establish the electrical conductivity of rocks which mainly consist of alkali feldspar and quartz. The EM model can be expressed as (Landauer 1952)

$$\sigma_{EM} = \frac{1}{4}\left\{\sigma_A(3f_A - 1) + \sigma_Q(3f_Q - 1). + \sqrt{\sigma_A(3f_A - 1) + \sigma_Q(3f_Q - 1) + 8\sigma_A\sigma_Q}\right\} \quad (9)$$

in this study where σ_A and σ_Q are the electrical conductivities of alkali feldspar and quartz, respectively, and f_A and f_Q are the their volume percentage, respectively.

The construction of electrical conductivity model of rocks is based on the following assumptions: (1) The effect of grain boundary on electrical conductivity of rocks, which often has very small contribution at high pressure, is assumed to be negligible; (2) the influence of water on the bulk electrical conductivity of rocks must be not considered because our samples are dry; (3) the very little portion of accessory minerals in rocks are neglected, as it has the least possibility of affecting the bulk electrical conductivity of rocks; (4) the two mineral phases, alkali feldspar and quartz, are supposed to be randomly distributed in rocks. On the basis of the rules above, we will establish the electrical conductivity of alkali feldspar granite, alkali feldspar quartz syenite, and alkali feldspar syenite, which are the typical and important rocks in the upper crust, at temperatures of 673–1,173 K and 1.0 GPa, and these rocks are shown in the QAP diagram for plutonic rocks in Fig. 8.

Since the electrical conductivity of alkali feldspar in this study satisfies the Arrhenius behavior as shown in Fig. 4, we use the parameters in Table 2 to extrapolate the electrical conductivity of alkali feldspar in temperature range of 673–873 K. For the electrical conductivity of quartz, although there have been many studies on the electrical conductivity of quartz, the data of Bagdassarov and Delépine (2004) are chosen because their experimental temperature, pressure, and method (AC impedance spectroscopy technique) are similar to ours. The most importance is that the electrical conductivity of single-crystal quartz shows very strong anisotropy as many publications reported (Verhoogen 1952; Jain and Nowick 1982; Wang et al. 2010). However, Bagdassarov and Delépine used polycrystalline quartz sample, which effectively avoids the effect of anisotropy. Additionally, although there will be a phase transition for quartz in temperature range of 673–1,173 K covered in our model, a large number of studies show that the electrical conductivity of quartz exhibits no abrupt change near the alpha–beta phase transition (Verhoogen 1952; Jain and Nowick 1982; Wang et al. 2010). Therefore, the effect of the α–β

Table 3 Fitting parameters obtained from the Eqs. (7) and (8) for electrical conductivity of alkali feldspar solid solutions

$X_{Na/(Na+K)}$	σ_0 (K·S/m)	ΔH_0 (eV)	α	β	γ
<0.5	35,237 ± 721	1.00 ± 0.01	0.40 ± 0.06	−0.23 ± 0.02	1.87 ± 0.03
>0.5	18,321 ± 367	0.92 ± 0.01	1.37 ± 0.16	−0.08 ± 0.01	1.00 ± 0.02

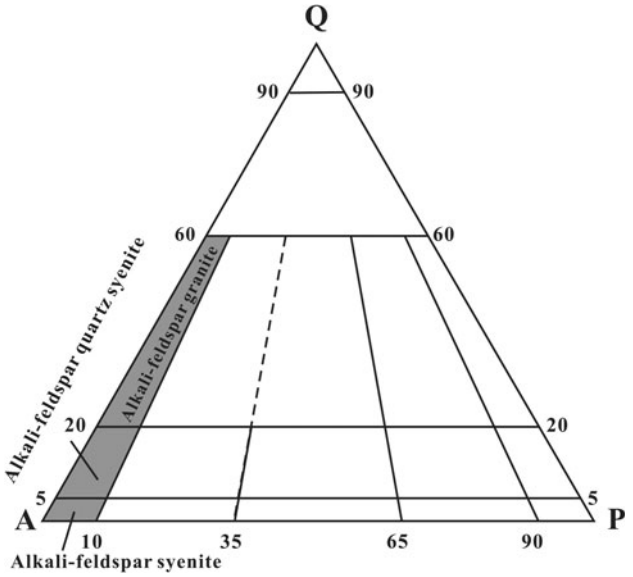

Fig. 8 Chosen rocks to calculate their electrical conductivity are shown in AQP diagram. The content of alkali feldspar and quartz in rocks can be directly read from the AQP diagram

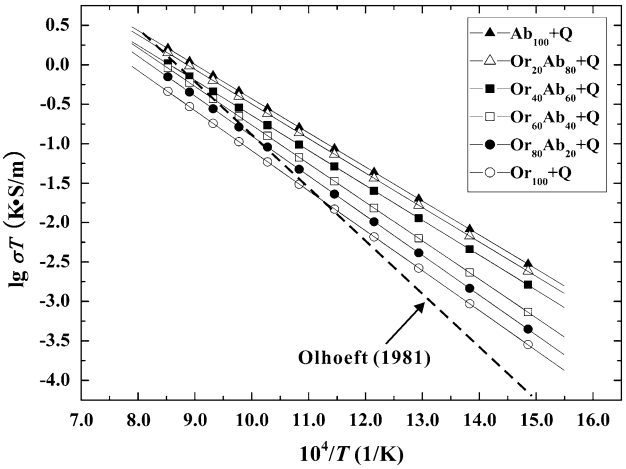

Fig. 9 Logarithmic conductivity (lg σT) of alkali feldspar granite consisting of 70 % alkali feldspar with different compositions and 30 % quartz against reciprocal temperature (1/K)) at 1.0 GPa. The *dashed line* shows the electrical conductivity of natural Westerly granite at room pressure measured by Olhoeft (1981)

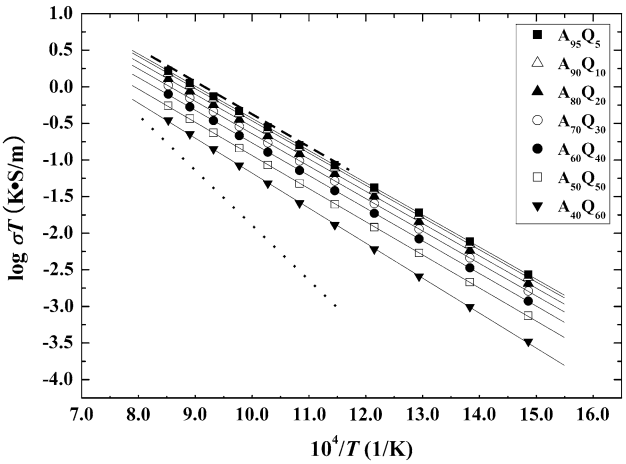

Fig. 10 Logarithmic conductivity (lg σT) of rocks with different volume percentage of quartz and alkali feldspar with the particular composition of $Al_{60}Or_{40}$ at 1.0 GPa against the reciprocal temperature (1/K). Also shown are data for $Al_{60}Or_{40}$ (*dashed line*) in this study and for quartz (*dotted line*) from Bagdassarov and Delépine (2004)

phase transition on the electrical conductivity of quartz is not taken into account. Based on the assumption and experimental data, we calculated the bulk electrical conductivity of alkali feldspar granite, alkali feldspar quartz syenite and alkali feldspar syenite. The results are shown in Figs. 9 and 10.

Figure 9 shows the logarithmic conductivity of alkali feldspar granite consisting of 70 % alkali feldspar with different chemical compositions and 30 % quartz against reciprocal temperature at 1.0 GPa. The results show that (1) the model electrical conductivities of alkali feldspar granite also satisfy the Arrhenius formula, namely, the electrical conductivity of alkali feldspar granite linearly increase with increasing temperature; (2) the electrical conductivity of alkali feldspar granite decreases with the decrease in albite content in alkali feldspar, which is similar to that of alkali feldspar solid solutions as shown in Fig. 4. Our calculated results are generally in accordance with those of dry Westerly granite in high-temperature region, but in low-temperature region, our results are slightly higher than those of Olhoeft (1981). The discrepancy can be attributed to the different mineralogical constituents of two rocks. As far as we know, the natural Westerly granite mainly consists of oligoclase, microcline, quartz, and biotite with minor muscovite (Tullis and Yund 1977). By contrast, our samples are composed of alkali feldspar (70 %) and quartz (30 %). In addition, the DC electrical conductivity of natural granite measured by Olhoeft (1981) is usually lower than the true values as we discussed above.

The logarithmic conductivity of rocks with different volume percentage of quartz and alkali feldspar with the composition of $Al_{60}Or_{40}$ at 1.0 GPa is plotted against the reciprocal temperature in Fig. 10. Since the electrical conductivity of quartz from Bagdassarov and Delépine (2004) is much lower than that of alkali feldspar in this study, the bulk conductivity of rocks remarkably decreases after quartz is added and reduces faster as the quartz content increases. However, in our model, the volume percentage of alkali feldspar in rocks is not less than 40 % which has been enough for alkali feldspar to form interconnected conduction network; hence, the bulk electrical

conductivity of these rocks is theoretically controlled by the more conductive alkali feldspar. Actually, our theoretical calculation results are consistent with the experimental values. Alvarez et al. (1978) had once measured the electrical conductivity of four igneous rocks with different composition at high temperature and found the electrical conductivity increases with the increase in the ratio of the albite to quartz. Parkhomenko (1982) also had done a lot of work on the relationship between the electrical conductivity of rocks and their minerals, chemical composition, and structure. His results showed that the electrical conductivity of acid and intermediate rocks such as granite and diorite decreased with the increasing content of quartz. His explanation is that the increase in SiO_2 content leads to the decrease in the sum of the alkaline oxide (e.g., CaO, K_2O, Na_2O) and the oxide of iron ($FeO + Fe_2O_3$), namely, the contributions of cations to the electrical conductivity reduce, which ultimately results in the decrease in electrical conductivity of these rocks. Our calculated results also show that the electrical conductivity of rocks decreases with the increase in the content of quartz and are in accordance with those of Alvarez et al. (1978) and Parkhomenko (1982).

Acknowledgments We thank Professors Hongfeng Tang and Hui Zhang for assistance in petrology, Wenqin Zheng for the use of microelectron probe, and two anonymous reviewers for their constructive comments. This research was financially supported by the Knowledge-Innovation Key Orientation Project of CAS (Grant Nos. KZCX2-YW-Q08-3-4 and KZCX2-YW-QN110) and NSF of China (Grant Nos. 40974051 and 40114079).

References

Alvarez R, Reynoso JP, Alvarez LJ, Martinez ML (1978) Electrical conductivity of igneous rocks: composition and temperature relations. Bull Volcanol 41:317–327

Bagdassarov NS, Delépine N (2004) α–β inversion in quartz from low frequency electrical impedance spectroscopy. J Phys Chem Solids 65:1517–1526

Bagdassarov NS, Maumus J, Poe B, Bulatov V (2004) Pressure dependence of Tg in silicate glasses from electrical impedance measurements. Phys Chem Glasses B 45:197–214

Bakhterev VV (2008) High temperature electric conductivity of some feldspars. Dokl Earth Sci 420:554–557

Beekmans N, Heyne L (1976) Correlation between impedance, microstructure and composition of calcia-stabilized zirconia. Electrochim Acta 21:303–310

Behrens H, Johannes W, Schmalzried H (1990) On the mechanisms of cation diffusion processes in ternary feldspars. Phys Chem Minerals 17:62–78

Christoffersen R, Yund RA, Tullus J (1983) Inter-diffusion of K and Na in alkali feldspars: diffusion couple experiments. Am Mineral 68:1113–1126

Constable S (1990) Electrical conductivity of olivine, a dunite, and the mantle. J Geophys Res 95:6967–6978

Dai L, Karato S (2009a) Electrical conductivity of orthopyroxene: implications for the water content of the asthenosphere. P Jpn Acad B Phys 85:466–475

Dai L, Karato S (2009b) Electrical conductivity of wadsleyite at high temperatures and high pressures. Earth Planet Sci Lett 287:277–283

Dai L, Karato S (2009c) Electrical conductivity of pyrope-rich garnet at high temperature and high pressure. Phys Earth Planet Inter 176:83–88

Dai L, Li H, Hu H, Shan S (2008) Experimental study of grain boundary electrical conductivities of dry synthetic peridotite under high-temperature, high-pressure, and different oxygen fugacity conditions. J Geophys Res 113:B12211

Dai L, Li H, Hu H, Shan S, Jiang J, Hui K (2012) The effect of chemical composition and oxygen fugacity on the electrical conductivity of dry and hydrous garnet at high temperatures and pressures. Contrib Mineral Petrol 163(4):689–700

Del Rio JA, Zimmerman RW, Dawe RA (1998) Formula for the conductivity of a two-component material based on the reciprocity theorem. Solid State Commun 106:183–186

Dowty E (1980) Crystal-chemical factors affecting the mobility of ions in minerals. Am Mineral 65:174–182

Duba A, Boland JN, Ringwood AE (1973) The electrical conductivity of pyroxene. J Geol 81:727–735

Dvorák Z, Schloessin HH (1973) On the anisotropic electrical conductivity of enstatite as a function of pressure and temperature. Geophysics 38:25–36

Eichler J, Lesniak C (2008) Boron nitride (BN) and BN composites for high-temperature applications. J Eur Ceram Soc 28(5):1105–1109

Eldin FME, Alaily NAE (1998) Electrical conductivity of some alkali silicate glasses. Mater Chem Phys 52:175–179

Farla R, Peach C, ten Grotenhuis SM (2010) Electrical conductivity of synthetic iron-bearing olivine. Phys Chem Minerals 37:167–178

Fuji-ta K, Katsura T, Tainosho Y (2004) Electrical conductivity measurement of granulite under mid- to lower crustal pressure-temperature conditions. Geophys J Int 157:79–86

Fuji-ta K, Katsura T, Matsuzaki T, Ichiki M, Kobayashi T (2007) Electrical conductivity measurement of gneiss under mid-to lower crustal P-T conditions. Tectonophysics 434:93–101

Guseinov AA, Gargatsev IO (2002) Electrical conductivity of alkaline feldspars at high temperatures. Izv Phys Solid Earth 38:520–523

Hashin Z, Shtrikman S (1962) A variational approach to the theory of the effective magnetic permeability of multiphase materials. J Appl Phys 33:3125–3131

Henderson P, Nolan J, Cunningham GC, Lowry RK (1985) Structural controls and mechanisms of diffusion in natural silicate melts. Contrib Mineral Petrol 89:263–272

Hirsch LM, Shankland TJ, Duba AG (1993) Electrical conductivity and polaron mobility in Fe-bearing olivine. Geophys J Int 114:36–44

Hu H, Li H, Dai L, Shan S, Zhu C (2011) Electrical conductivity of albite at high temperatures and high pressures. Am Mineral 96:1821–1827

Huebner JS, Dillenburg RG (1995) Impedance spectra of hot, dry silicate minerals and rock: qualitative interpretation of spectra. Am Mineral 80:46–64

Jain H, Nowick AS (1982) Electrical conductivity of synthetic and natural quartz crystals. J Appl Phys 53:477–484

Jones A, Islam MS, Mortimer M, Palmer D (2004) Alkali ion migration in albite and K-feldspar. Phys Chem Minerals 31:313–320

Khitarov N, Slutskiy A (1965) The effect of pressure on the melting temperatures of albite and basalt (based on electroconductivity measurements). Geochem Int 2:1034–1042

Landauer R (1952) The electrical resistance of binary metallic mixtures. J Appl Phys 23:779–784

Li H, Xie H, Jie G, Zhang Y, Xu Z (1999) In situ control of oxygen fugacity at high temperature and high pressure. J Geopyhs Res 104:439–451

Lin TH, Yund RA (1972) Potassium and sodium self-diffusion in alkali feldspar potassium and sodium self-diffusion in alkali feldspar. Contrib Mineral Petrol 34:177–184

Liu L, Gorsey AE (2007) High-pressure phase transitions of the feldspars, and further characterization of lingunite. Int Geol Rev 49:854–860

Liu W, Du J, Yong Y, Bai P, Wang C (2003) Correction of temperature gradient in sample cell of pulse transmission experimental setup on multi-anvil high pressure apparatus. Chin J High Pressure Phys 17:95–100

Maury R (1968a) Conductivilite electrique des tectosilicates. I. Methode des resultats experimentaux. Bulletin de la Societe Francaise de Mineralogie et Cristallographie 91:267–278

Maury R (1968b) Conductivilite electrique des tectosilicates. II. Discussion des resultats. Bulletin de la Societe Francaise de Mineralogie et Cristallographie 91:355–366

Mizutani H, Kanamori H (1967) Electrical conductivities of rock-forming minerals at high temperatures. J Phys Earth 15:25–31

Ni H, Keppler H, Manthilake M, Katsura T (2011) Electrical conductivity of dry and hydrous $NaAlSi_3O_8$ glasses and liquids at high pressures. Contrib Mineral Petrol 162(3):501–513

Noritomi K (1955) Studies on the change of electrical conductivity with temperature of a few silicate minerals. Science Reports Tohoku Univ Ser 5(6):119–126

Ohashi Y (1976) Lattice energy of some silicate minerals and the effect of oxygen bridging in relation to crystallization sequence. Carnegie Inst Wash Year Book 75:644–648

Olhoeft G (1981) Electrical properties of granite with implications for the lower crust. J Geopyhs Res 86(B2):931–936

Omura K, Kurita K, Kumazawa M (1989) Experimental study of pressure dependence of electrical conductivity of olivine at high temperatures. Phys Earth Planet Inter 57:291–303

Parkhomenko E (1982) Electrical resistivity of minerals and rocks at high temperature and pressure. Rev Geophys 20:193–218

Piwinskii AJ, Duba A (1974) High temperature electrical conductivity of albite. Geophys Res Lett 1:209–211

Piwinskii AJ, Duba A, Ho P (1977) The electrical conductivity of low and high albite throughout its melting interval at 100 kPa. Can Mineral 15:196–197

Poe B, Romano C, Nestola F, Smyth JR (2010) Electrical conductivity anisotropy of dry and hydrous olivine at 8 GPa. Phys Earth Planet Inter 181:103–111

Roberts JJ, Tyburczy JA (1991) Frequency dependent electrical properties of polycrystalline olivine compacts. J Geopyhs Res 96:16205–16222

Roberts JJ, Tyburczy JA (1993) Impedance spectroscopy of single and polycrystalline olivine: evidence for grain boundary transport. Phys Chem Minerals 20:19–26

Romano C, Poe BT, Kreidie N, McCammon CA (2006) Electrical conductivities of pyrope-almandine garnets up to 19 GPa and 1700 °C. Am Mineral 91(8–9):1371

Schulgasser K (1976) Relationship between single-crystal and polycrystal electrical conductivity. J Appl Phys 47:1880–1886

Seifert KF, Will G, Voigt R (1982) Electrical conductivity measurements on synthetic pyroxenes $MgSiO_3$-$FeSiO_3$ at high pressures and temperatures under defined thermodynamic conditions. In: Schreyer W (ed) High-pressure researches in geoscience. Schweizerbart'sche, Stuttgart, pp 419–432

Shan S, Wang R, Guo J, Li H (2007) Pressure calibration for the sample cell of YJ-3000t multi-anvil press at high temperature and high pressure. Chin J High Pressure Phys 21:367–372

Shankland T, Duba A (1990) Standard electrical conductivity of isotropic, homogeneous olivine in the temperature range 1200–1500 °C. Geophys J Int 103:25–31

Tullis J, Yund RA (1977) Experimental deformation of dry Westerly granite. J Geopyhs Res 82(36):5705–5718

Tyburczy JA, Fisler DK (1995) Electrical properties of minerals and melts. In: Ahrens TJ (ed) Mineral physics and crystallography: a handbook of physical constants, Ref. Shelf, vol 2. AGU, Washington, DC, pp 185–208

Verhoogen J (1952) Ionic diffusion and electrical conductivity in quartz. Am Mineral 37:637–655

Wang D, Li H, Yi L, Matsuzaki T, Yoshino T (2010) Anisotropy of synthetic quartz electrical conductivity at high pressure and temperature. J Geopyhs Res 115:B09211

Xu Y, Shankland TJ, Poe BT (2000) Laboratory-based electrical conductivity in the Earth's mantle. J Geopyhs Res 105:827–865

Yang X (2012) Orientation-related electrical conductivity of hydrous olivine, clinopyroxene and plagioclase and implications for the structure of the lower continental crust and uppermost mantle. Earth Planet Sci Lett 317–318:241–250

Yang X, Heidelbach F (2012) Grain size effect on the electrical conductivity of clinopyroxene. Contrib Mineral Petrol 163(6):939–947

Yang X, Keppler H, McCammon C, Ni H (2012) Electrical conductivity of orthopyroxene and plagioclase in the lower crust. Contrib Mineral Petrol 63:33–48

Yoshino T (2010) Laboratory electrical conductivity measurement of mantle minerals. Surv Geophys 31:163–206

Yoshino T, Katsura T (2009) Effect of iron content on electrical conductivity of ringwoodite, with implications for electrical structure in the transition zone. Phys Earth Planet Inter 174(1–4):3–9

Yoshino T, Matsuzaki T, Shatskiy A, Katsura T (2009) The effect of water on the electrical conductivity of olivine aggregates and its implications for the electrical structure of the upper mantle. Earth Planet Sci Lett 288(1–2):291–300

Yoshino T, Ito E, Katsura T, Yamazaki D, Shan S, Guo X, Nishi M, Higo Y, Funakoshi K (2011) Effect of iron content on electrical conductivity of ferropericlase with implications for the spin transition pressure. J Geopyhs Res 116(B4):B04202

Yoshino T, Shimojuku A, Shan S, Guo X, Yamazaki D, Ito E, Higo Y, Funakoshi K (2012) Effect of temperature, pressure and iron content on the electrical conductivity of olivine and its high-pressure polymorphs. J Geopyhs Res 117(B8):B08205

Zhong H, Zhu WG, Hu RZ, Xie LW, He DF, Liu F, Chu ZY (2009) Zircon U-Pb age and Sr-Nd-Hf isotope geochemistry of the Panzhihua A-type syenitic intrusion in the Emeishan large igneous province, southwest China and implications for growth of juvenile crust. Lithos 110:109–128

Zhou L, Guo J, Liu B, Li L (2001) Structural state of adularia from Hishikari, Japan. Chinese Sci Bull 46:950–953